Expanded scaling relations for locomotion in sloped or cohesive granular beds

Qiong Zhang, Stephen Townsend, and Ken Kamrin*
Department of Mechanical Engineering, MIT, Cambridge, Massachusetts 02139, USA

(Received 10 March 2020; accepted 28 September 2020; published 3 November 2020)

Dynamic similarity, while commonly applied in fluid systems, has recently been extended to locomotion problems in granular media. The previous work was limited to locomotors in cohesionless, flat beds of grains under the assumption of a simple frictional fluid rheology. However, many natural circumstances involve beds that are sloped or composed of cohesive (e.g. damp or powdery) grains. Here we derive expanded scaling relations inclusive of these phenomena. To validate the proposed scalings, we perform discrete element method simulations with inclined beds and cohesive grains using rotating "wheels" of various shape families, sizes, and loading conditions in accord with the proposed scaling laws. The data show a good agreement between scaled tests, suggesting the usage of these scalings as a potential design tool for off-road vehicles and extraplanetary rovers and as an analysis tool for biolocomotion in soils.

DOI: 10.1103/PhysRevFluids.5.114301

I. INTRODUCTION

Locomotion problems in granular media have been studied in experiments for various purposes from understanding the nature of animals [1–3], to guiding the design of vehicles on unprepared ground [4], and even planetary explorations [5,6]. Fully resolved simulations using the discrete element method (DEM) [7,8] have also been employed, especially in the cases where detailed information such as the flow field near the locomotor is of interest. In practice, engineering terramechanics models [9–11] are developed for the design of vehicles which typically require many empirical parameters. Resistive force theory [12,13], though initially proposed for viscous fluids, has also shown efficacy in modeling locomotion of generic locomotors in granular media [14,15].

Inspired by dynamic similarity in fluids problems, one option is to seek out scaling laws for locomotion based on a presumed granular constitutive relation. Many complexities in granular rheology are known to exist, including history-dependent effects [16–18], anisotropy [19], hysteresis [20], rate-dependent effects [21,22], nonlocal effects [23,24], and relaxational dynamics [25]. Including all these effects in a continuum model would produce a very complicated and not particularly robust set of scaling relations. In Ref. [26] scaling relations for locomotion in flat beds of dry granular material were considered based on a model that sets aside most of these complexities and assumes only a tension-free frictional rheology, which is independent of grain size. Despite using a simplified model, the scaling relations obtained in Ref. [26] were shown to describe many features of locomotion in dry flat granular beds in a number of experiments and DEM simulations. However, terrains in nature are frequently sloped (e.g., hills, piles, dunes) and the grains may be cohesive, typically due to moisture or attraction from van der Waals or electrostatic forces, giving rise to novel locomotive dynamics [27,28]. How or if scaling relations extend under these circumstances

*kkamrin@mit.edu

has remained unclear. Furthermore, since the previous scaling law was shown to be effective under variations of gravity, if an extended scaling relation could be found, it could lead to novel protocols for modeling extraplanetary rovers by way of experiments performed on earth that properly scale the gravity and essential frictional/cohesive soil character of the target environment.

In this work, extended scaling relations for basic locomotive observables, such as power expenditure of the locomotor and its traveling velocity, are proposed for use in inclined and/or cohesive granular beds. For verification, DEM simulations are performed using locomotors of various sizes and three different locomotor shapes (triangle, rectangle, and hexagon) along with a variety of mass loadings, rotation speeds, and gravities. We show the proposed scalings are satisfied in separate studies of sloped beds and cohesive grains.

II. DIMENSIONAL ANALYSIS

Our scaling analysis begins by supposing a simple continuum model for the granular media and analyzing its dimensional consequences. First, the media satisfies momentum balance

$$\rho \dot{\boldsymbol{v}} = \boldsymbol{\nabla} \cdot \boldsymbol{\sigma} + \rho \boldsymbol{b}$$

where $\boldsymbol{v}$ is the velocity of a material point, $\boldsymbol{\sigma}$ the Cauchy stress tensor, ρ the density of the material, and $\boldsymbol{b}$ the specific body force. We consider a constitutive relation that assumes wherever the density is below a critical value, ρ_0, the material is disconnected and thus stress-free (i.e., $\boldsymbol{\sigma} = \mathbf{0}$ when $\rho < \rho_0$). Alternatively, in the dense state, which is described as when $\rho = \rho_0$, we presume a frictional and cohesive rheology, which can be concisely summarized with the system of constraints below:

$$\begin{aligned} \dot{\rho}(C_2 + p) = 0 \quad &\text{and} \quad C_2 + p \geqslant 0 \quad \text{and} \quad \dot{\rho} \leqslant 0, \\ f_y \dot{\gamma} = 0 \quad &\text{and} \quad f_y = \tau - \mu_s p - C_1 \leqslant 0 \quad \text{and} \quad \dot{\gamma} \geqslant 0, \end{aligned}$$

where p is the pressure, $\dot{\gamma}$ the shear rate, τ the shear stress, and μ_s the material critical friction coefficient [29]. C_1 is the cohesive shear stress that must be overcome in order to plastically shear the material at zero pressure [30–33], and $-C_2$ is the hydrostatic stress necessary to detach the material in uniform expansion. In words, the first equation above states that material exiting the dense state ($\dot{\rho} < 0$) does so when its pressure becomes critical ($p = -C_2$), otherwise material that is above the expansion criterion ($p > -C_2$) can flow only incompressibly ($\dot{\rho} = 0$). The second equation above states that either material is shearing and the stress satisfies $f_y = 0$, or the material is not shearing and the stress is subyield, $f_y < 0$. For noncohesive grains, C_1, C_2 are zero. For cohesive grains, C_1 and C_2 both manifest from the same microscale source, cohesive bonds at the grain contacts, so we assume both C_1 and C_2 are expressible in terms of a common characteristic cohesion stress, which we denote as σ_c.

The constitutive model is free of particle size effects, which is justifiable as long as the length scale of the locomotor and sinkage is much larger than the grain scale [23,34,35] including possible grain-size-based cohesion length scales. Also, note that the constitutive equations above are rate-independent; the inertial number $I \sim \dot{\gamma}/\sqrt{p}$ [21] is deemed too small to affect the flow resistance. Indeed, the dependence of shear stress on rate is typically low for granular intrusion problems, even rapid ones, because high pressure develops against the intruding surface, which counters the large shear rate in the inertial number definition. For example, Ref. [36] modeled the same impact problems using both a rate-dependent constitutive model and a rate-independent model and found the difference in predicted intruder motion to be rather small (<10%) in terms of traveling depth and time. Even though the particle inertial time scale is not particularly relevant to the intruder's trajectory, this does not imply that all impact observables are free of influence from material timescales. For example, grain elasticity and intrusion speed have been shown in experiments [37] to strongly affect the growth rate of force chains surrounding an intruder.

With the constitutive model just described, we next infer scaling relations for locomotion and check how well they hold against a number of DEM simulations. In so doing, this study is also a *de*

facto check on the validity of using the above basic continuum assumptions for these problems. We perform a dimensional analysis similar to that in Ref. [26]. For a wheel having large out-of-plane thickness D_W and characteristic in-plane length L, one can nondimensionalize the driving inputs and constitutive parameters to express the velocity V of the wheel and power P expended by the wheel as follows:

$$\left[\frac{P}{Mg\sqrt{Lg}}, \frac{V}{\sqrt{Lg}}\right] = \Psi\left(\sqrt{\frac{g}{L}}t, f, \frac{g}{L\omega^2}, \frac{\rho_0 D_W L^2}{M}, \mu_s, \mu_w, \frac{\rho_0 g L}{\sigma_c}, \theta\right) \tag{1}$$

for some two-output scaling function Ψ. Here t is time, the gravitational acceleration is g, the inclination of the bed relative to the direction of gravity is θ, the mass of the wheel is M, the rotational speed is ω, the shape of the wheel is represented by a set f, and μ_w is the friction coefficient of the wheel-bed interface. Each set of scaling tests below utilizes a fixed granular material and fixed wheel roughness so μ_s and μ_w can be absorbed into the undetermined Ψ function.

We study the validity of the above relation by splitting it into two sets of cases, which we shall analyze separately. We consider wheels traveling on inclined beds of noncohesive particles, where the dimensionless number $\frac{\rho_0 g L}{\sigma_c}$ is not involved. Thus the relation becomes

$$\left[\frac{P}{Mg\sqrt{Lg}}, \frac{V}{\sqrt{Lg}}\right] = \tilde{\Psi}_1\left(\sqrt{\frac{g}{L}}t, f, \frac{g}{L\omega^2}, \frac{\rho_0 D_W L^2}{M}, \theta\right). \tag{2}$$

We also consider the case of wheels traveling on horizontal beds of cohesive granular media. Here we can take away θ and the relation becomes

$$\left[\frac{P}{Mg\sqrt{Lg}}, \frac{V}{\sqrt{Lg}}\right] = \tilde{\Psi}_2\left(\sqrt{\frac{g}{L}}t, f, \frac{g}{L\omega^2}, \frac{\rho_0 D_W L^2}{M}, \frac{\rho_0 g L}{\sigma_c}\right). \tag{3}$$

III. NUMERICAL EXPERIMENTS

In order to test the proposed scaling relations, traveling wheels of different sizes and different shapes in different operating conditions are numerically simulated on horizontal granular beds of cohesive particles as well as inclined granular beds of noncohesive particles using the open source software LAMMPS [38]. In all our numerical experiments, the granular beds are made of particles with a mean diameter of $\bar{d} = 0.635$ mm and the polydispersity is 20%. The solid density of grains is 2500 kg/m^3, close to the density of quartz. For noncohesive granular beds, the contact model is Hooke's law in both normal and tangential directions, with damping in the normal direction and a frictional sliding coefficient of 0.4 [39,40]. The stiffness k is set large enough that the hard particle limit is satisfied everywhere in the bed—that is, $p_b\bar{d}/k < 10^{-4}$, where p_b is the pressure in the bed due to the weight and motion of the material—and the damping corresponds to a restitution coefficient $e = 0.1$. The same values of the particle parameters have been used in previous studies [26,41].

For the cohesive particles, there are a few cohesive granular interaction models such as capillary models [42,43], van der Waals interactions [44], the powder chemistry model [45], the liquid bridging model [46], and DLVO theory [47]. In our simulations, as used in other researchers' work on cohesive particles [44,48], cohesive particles have an extra Lennard-Jones potential to enable medium range attraction, with the help of the built-in function *lj/cut* in LAMMPS. The radius at which distance the potential is minimum is set to be $\bar{d}$ and the potential is calculated within a cutoff of $2.5\bar{d}$. The depth of the potential well is 2×10^{-9} J.

Our choice to use a fixed granular material for all scaled locomotion tests is for practical purposes, as it would be difficult in reality to have to "manufacture new sand" in order to utilize a scaling relation.

Because the scaling purports to apply to arbitrary wheel shapes, we consider three different shapes in this study: equilateral triangular wheels, rectangular wheels, and regular hexagonal wheels. All wheels are composed of particles having a uniform diameter $d_0 = 0.8$ mm rigidly

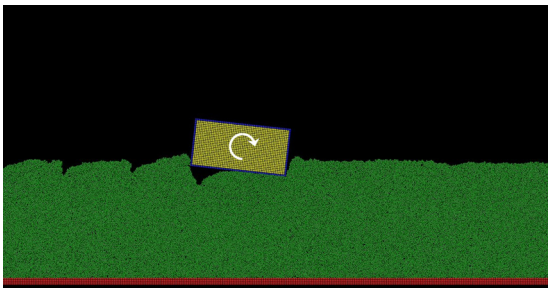

FIG. 1. Example simulation system—case of a rectangular wheel in cohesive grains pictured. A wheel comprising rigidly connected yellow inner particles and blue particles on the edge is given a fixed rotation speed, which causes it to travel to the right. The particles in the bed are shown in green, while the red particles at the bottom are fixed. The pictured domain width is about half of that of the whole simulated domain.

connected to each other. The characteristic in-plane size L of the triangular and hexagonal wheels are represented by the side lengths, while for the rectangular wheels (aspect ratio 2:1) L is represented by the long side length. The mechanical properties of the outer layers (single or double layers) of the wheel particles are set to be the same as the particles in the granular bed to maintain a common wheel-grain and grain-grain contact interaction, while the density of the inner layers of the wheel particles can be tuned accordingly to scale the mass of the wheel in the study. The rotational velocity of the wheel is prescribed about the wheel's geometric center, and the particles constituting the wheel move as a rigid body. When studying locomotion in a cohesive granular bed, the outer particles of the wheel also interact with the bed particles via the Lennard-Jones potential described above.

The numerical experiments are quasi-3D (see Fig. 1) in the sense that the simulated domain has a depth of d_0 into the page (y direction) and periodic boundary conditions are applied in the y direction, allowing the bed particles with a mean diameter $\bar{d} \sim 0.79d_0$ to move out of plane. Hence, the simulation represents a "thick" wheel driving on a granular bed. Periodic boundary conditions are also applied in the x direction (wheel traveling direction). The bottom of the bed is made of fixed particles, representing a no-slip boundary condition. In the simulations with horizontal beds, the gravity points vertically downward. Tilted beds are treated by tilting the gravity vector.

IV. SCALING LAW FOR WHEELS ON INCLINED BEDS OF NONCOHESIVE GRAINS

The numerical simulations of wheels traveling on inclined beds of noncohesive particles consist of three groups corresponding to three different shapes: triangle, rectangle (aspect ratio 2:1), and hexagon. Each group adopts a set of three wheels of identical shape but different sizes or operating parameters: we denote them A, B, and C, as shown in Table I, where the value of the parameters are shown in Table II with the wheel particle size $d_0 = 0.8$ mm. The parameters of the wheels are

TABLE I. Parameters of the wheels, in each group of the same shape, tested on inclined beds of noncohesive particles at varying angles. The numerical values can be obtained using Table II.

Wheel	Size	M/D_W	ω	g
A	L_1	M_1	ω_1	g_1
B	L_1	M_1	$2\omega_1$	$4g_1$
C	k_1L_1	$k_1^2M_1$	$\omega_1/\sqrt{k_1}$	g_1

TABLE II. Value of the parameters for different wheel shapes, tested on inclined beds of noncohesive particles at varying angles.

Shape	L_1/d_0	k_1	M_1 (kg m^{-1})	ω_1 (rps)	g_1 (m/s^2)
Triangle	36	3/2	0.56	1	9.8
Rectangle	36 (length)	3/2	1.09	1	9.8
Hexagonal	18	4/3	0.77	1	9.8

designed according to Eq. (2) such that $g/L\omega^2$ and $\rho_0 D_W L^2/M$ are fixed across all wheels sharing a common shape.

The range of scaled tests we perform are controlled by the following simulation constraints. The computational cost scales quadratically with the size of the wheel for each time step, and the number of the time steps needed scales with the square root of the wheel size, which places an upper limit on the sizes of the tested wheels. At the same time, the wheels also must be large enough to ensure removal of grain-size effects (i.e., ensure a sinkage of at least a few particle diameters). The rotation velocity is limited to avoid kicking the particles so violently that they eject across the periodic boundary and hit the wheel from the other side. The rotation velocity also cannot be too small, or the simulation time required will be prohibitive.

Each set of three wheels are tested with four different angles between the traveling direction and the gravity: $\theta = 85^\circ$ (downhill), 95° (uphill when $\theta > 90^\circ$), 100°, and 105°. Due to the periodic boundary conditions in the traveling direction and the finite depth of the granular bed, the angles are constrained to a range that permits the bed to be static in the absence of a wheel, and to ensure that any flows set off due to impact by the moving wheel do not cause grains to pass through the periodic boundary and hit the front of the wheel, nor produce divots that expose or come close to the bottom wall of the bed.

First we present detailed results of the rectangular wheel simulations. Snapshots of those simulations at a fixed value of $\tilde{t}$ are compared in Fig. 2. It can be seen that for each tilt angle θ, the footprint and impression patterns of the three wheel cases (A, B, and C) are geometrically similar, which is a first indication that the scaling relations proposed are indeed scaling the relevant physics. More quantitatively, the dimensionless power $\tilde{P} = \frac{P}{Mg\sqrt{Lg}}$ and traveling velocity $\tilde{V} = \frac{V}{\sqrt{Lg}}$ as a function of dimensionless time $\tilde{t} = t\sqrt{g/L}$ are shown in Fig. 3, comparing the set of three rectangle wheels on beds of noncohesive particles at different angles θ. The dimensionless power and traveling velocity of the three wheels show strong agreement, supporting the proposed scaling relation for driving up (or down) inclined terrains. More specifically, within the set of the three wheels, wheels A and C are under the same magnitude of gravity, whereas wheel B is under a different gravity magnitude. This suggests the potential of the scaling law to be applied to locomotion in extraplanetary terrains.

The dimensionless power and traveling velocity of the rectangular wheels can be further averaged in each case and then plotted as a function of inclination angle as shown in Fig. 4, in comparison with the counterparts of different shapes. The data are averaged over a distance of at least five wheel "diameters" (maximum length across the wheel) on a virgin bed surface in steady state. The scaling relation works well through different shapes, covering a range of inclination angles from uphill locomotion to downhill.

We also notice that the smaller triangle wheels (A and B) consume less power than the prediction ($\sim$10% less). This effect may be a result of size effects in granular flow rheology since the corners of the triangular wheels are sharp, causing penetration widths that compete with the grain size. The granular bed performs stronger (more difficult to deform) when the interaction occurs at limited contacts and in thin layers, which makes the smaller triangular wheels prone to sink slightly less, so that driving over the surface requires less power. Similar size effects were also observed when we tried "bar wheels" (elongated rectangles with an aspect ratio of 9:1 with the short edges no longer than $6d_0$). As the size of the wheel becomes much larger than the grain size (low aspect ratio

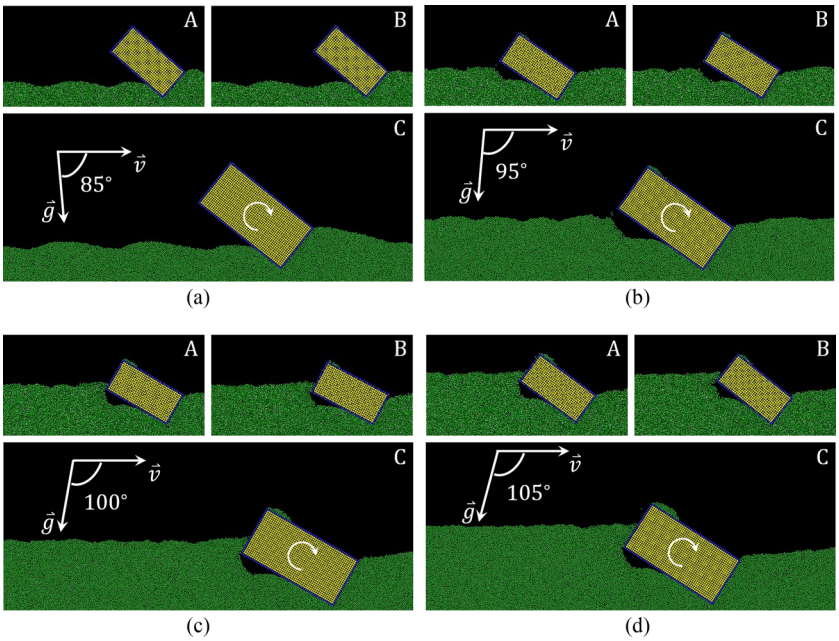

FIG. 2. For each of panels (a)–(d), snapshots are shown of rectangular wheels at the same dimensionless time driving in noncohesive particle beds of a particular tilt angle θ. The subfigures correspond to the supposed scale-equivalent test cases A, B, and C. The value of θ is (a) 85°, (b) 95°, (c) 100°, and (d) 105°. The wheels spin clockwise and travel to the right. $\tilde{t} \sim 82, 118, 81, 127$ for the four $\vec{g}$ angles, respectively.

rectangles shown here) and corners less sharp (hexagons), the size effect diminishes and the scaling law works well. The notion that grain-size effects make "smaller act stronger" in granular media is confirmed by experiments [20,49,50] and has been explained with nonlocal (grain-size-dependent) rheologies [23,34,51–54].

V. SCALING LAWS FOR COHESIVE GRAINS

To study the scaling relation on beds of cohesive particles, we have tested a set of three triangular wheels, three rectangular wheels, as well as three hexagonal wheels for generality. Dimensionless groups $g/L\omega^2$, $\rho_0 D_W L^2/M$, and $\rho_0 g L/\sigma_c$ are controlled and the design of the wheels can be found in Table III, where the parameters that are picked (see Table IV) produce reasonable wheel sinkages in the simulated domain.

Figure 5 shows snapshots of the simulations at the same dimensionless time. The "footprint" patterns left by wheels of the same shape but differing size show geometric similarity, a signature of the underlying scaling. Indeed, when the dimensionless wheel shapes are fixed (same f) and

TABLE III. Parameters of the wheels, in each group of the same shape, tested on horizontal beds of cohesive particles. The numerical values can be obtained using Table IV.

Wheel	Size	M/D_W	ω	g
Small	$k_2 L_2$	$k_2^2 M_2$	ω_2/k_2	g_2/k_2
Medium	L_2	M_2	ω_2	g_2
Large	$k_3 L_2$	$k_3^2 M_2$	ω_2/k_3	g_2/k_3

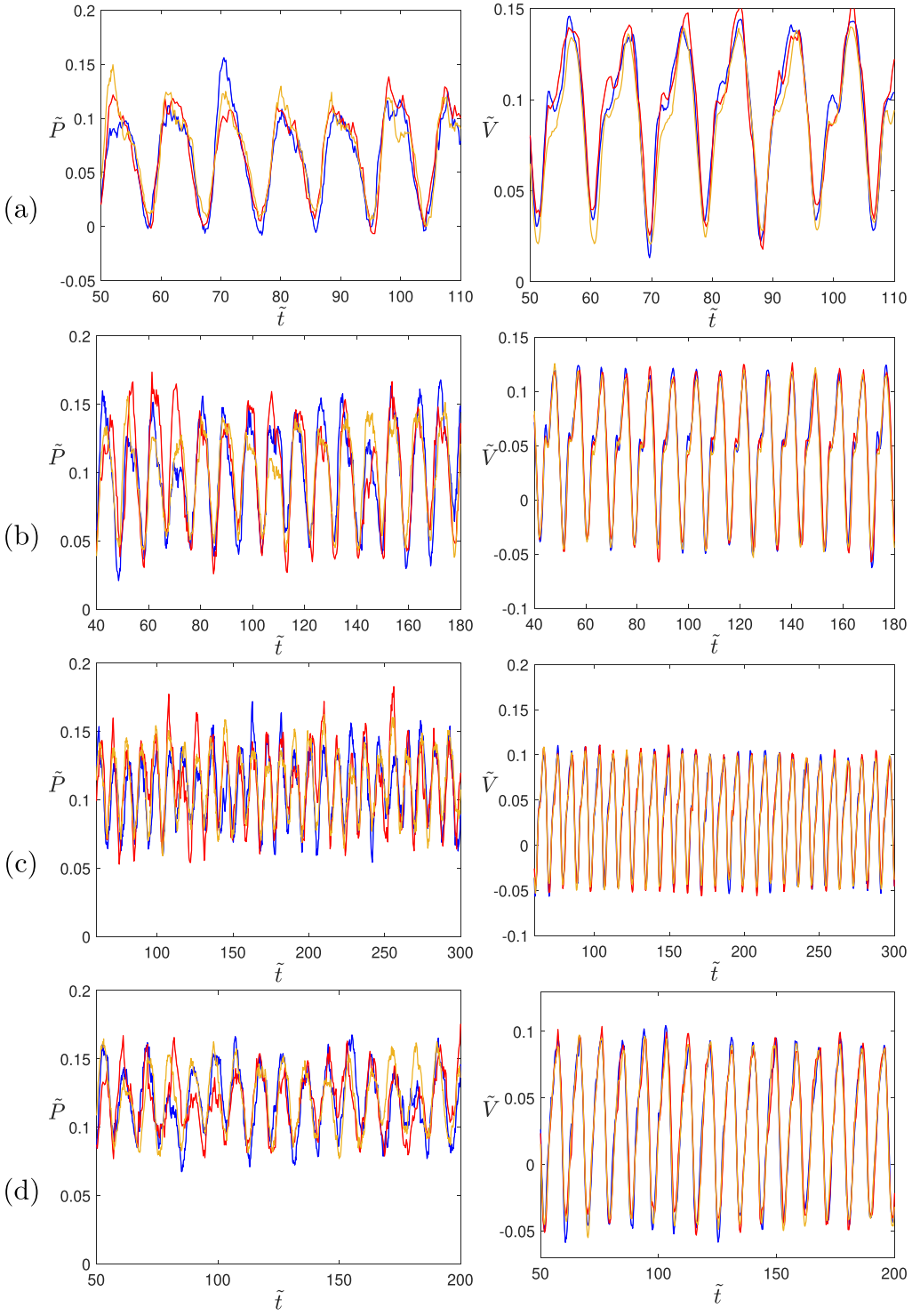

FIG. 3. Dimensionless power and traveling velocity comparisons of a set of three rectangle wheels on beds of noncohesive particles, with the angle θ between the traveling direction and the gravity (a) $\theta = 85^\circ$, (b) $\theta = 95^\circ$, (c) $\theta = 100^\circ$, (d) $\theta = 105^\circ$. Blue curves stand for case A, red for case B, and yellow for case C.

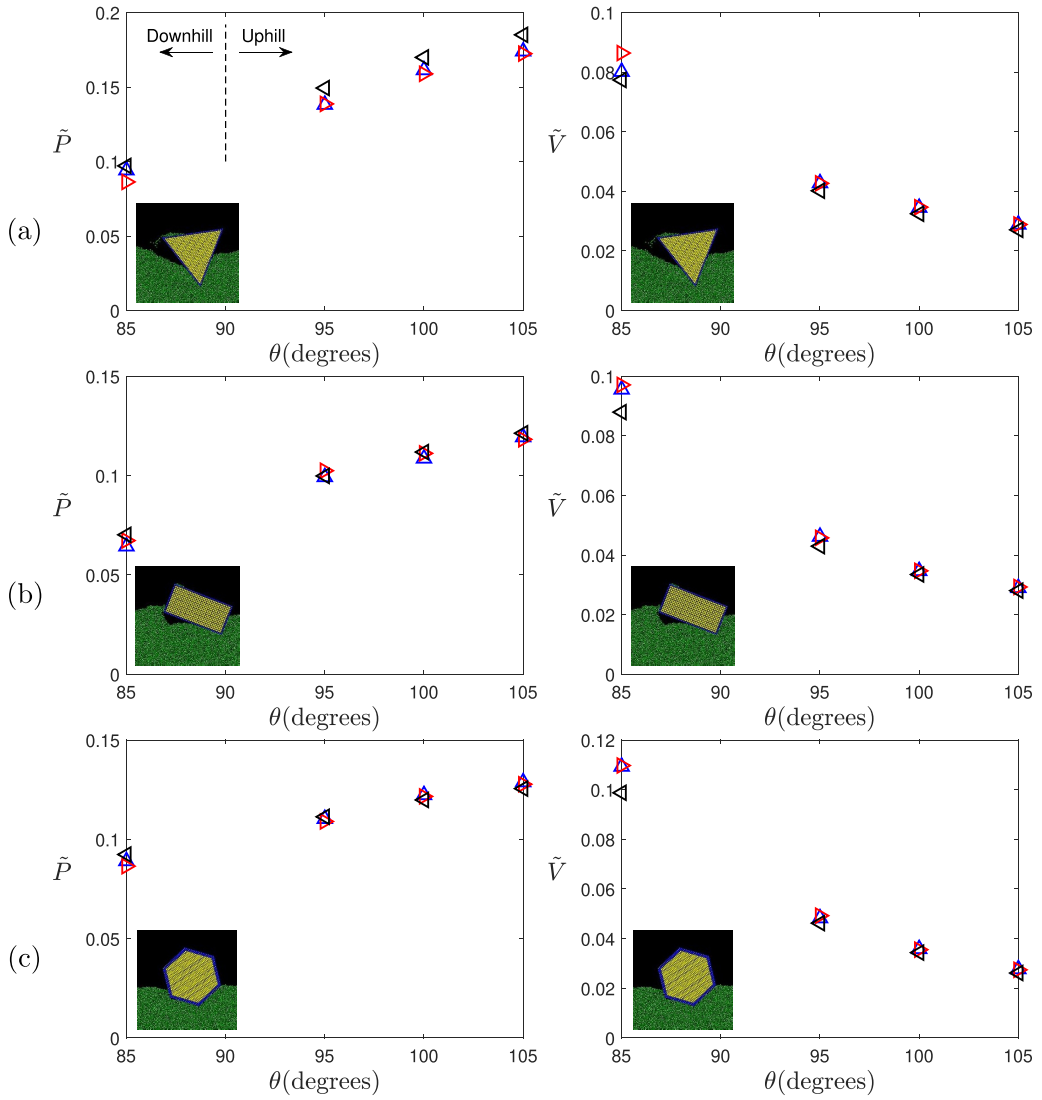

FIG. 4. Averaged dimensionless power and traveling velocity comparisons of (a) triangular wheels, (b) rectangular wheels, and (c) hexagonal wheels, at different inclined angles. Case A represented by blue markers, case B red, and case C black.

dimensionless groups $g/L\omega^2$, $\rho_0 D_W L^2/M$, $\rho_0 gL/\sigma_c$ are controlled to be the same, the power P and traveling velocity V appear to scale as in Eq. (3), as evidenced in Fig. 6. Both the triangular and rectangular wheels' dimensionless power and velocity as functions of dimensionless time match well, respectively. The hexagonal wheels have noisier time-dependent profiles, but the time-averaged values match best among all the tested shapes: $\tilde{P}$ within a difference of 1.0% and $\tilde{V}$ within a difference of 6.0% relative error with respect to the mean values of the time-averaged power and velocity, whereas the relative error of power and velocity is within 2.9% and 8.4% for rectangle wheels and 7.5% and 7.7% for triangle wheels. The scaling relation seems to be more robust to sharp corners; it appears the triangular wheels scale better in cohesive versus noncohesive particles.

TABLE IV. Value of the parameters for different wheel shapes on beds of cohesive particles.

Shape	L_2/d_0	k_2	k_3	M_2 (kg m^{-1})	ω_2 (rps)	g_2 (m/s^2)
Triangle	36	2/3	3/2	0.57	1	9.8
Rectangle	36 (length)	2/3	3/2	0.54	1	9.8
Hexagonal	18	2/3	4/3	0.77	1	9.8

Due to the cohesive nature of the particles, the gravity g and the characteristic length L produce the dimensionless group $\rho_0 gL/\sigma_c$. Observe that when the granular material and gravity are fixed, this group can stay fixed only if L is unchanged. Conversely, a test in one gravity to predict behavior in another comes with a specific size-scaling rule. For example, to test a Mars rover on Earth in a soil matching the behavior of Martian soil, the dimensionless group $\rho_0 gL/\sigma_c$ dictates that the size of the wheel to be tested on the Earth should be scaled to $(g_{\text{earth}}/g_{\text{mars}})^{-1} = 0.38$ times the size of the one intended for Mars. Other testing parameters can be decided by matching the dimensionless numbers in Eq. (3). Besides investigations involving variations in gravity, the scaling of wheel size in cohesive grains is also possible if one is able to directly control and vary the granular cohesion stress, σ_c, which would presumably require control over the physical mechanism causing particle attraction (e.g., water content, charging, solvent chemistry, or particle coating [55]).

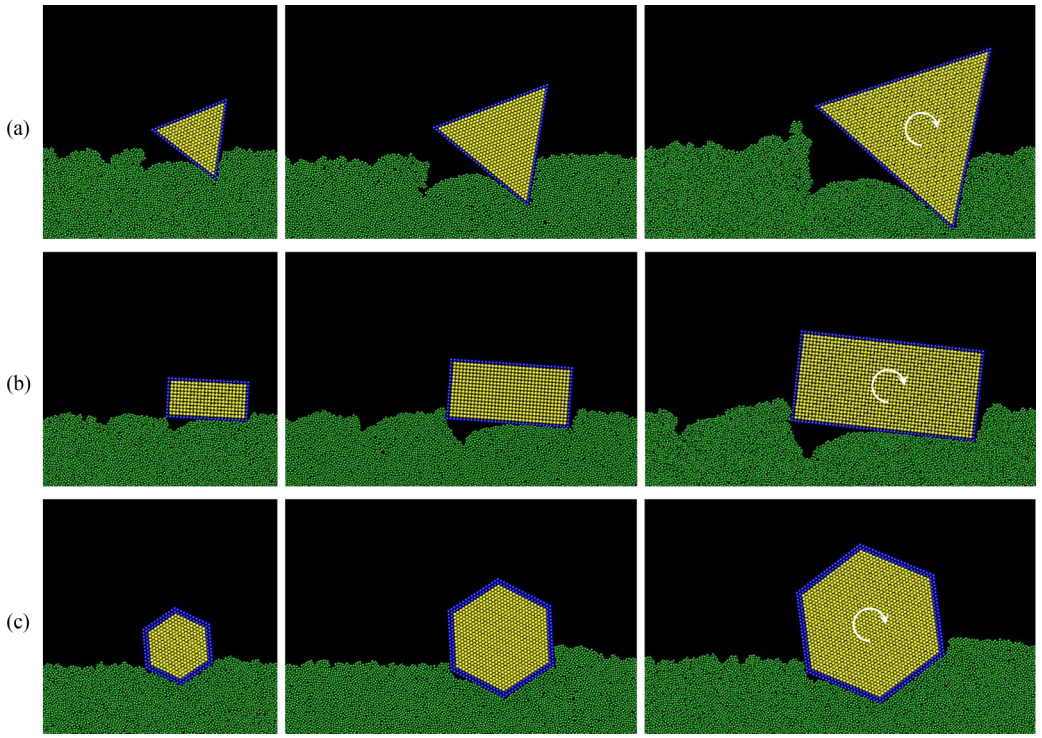

FIG. 5. Snapshots at the same $\tilde{t}$ of the differently shaped/sized wheels in horizontal cohesive particle beds: (a) triangular wheels, (b) rectangular wheels and (c) hexagonal wheels. All tests use the same DEM grains. Different wheel sizes are compared in different columns: small in the first column from the left, medium in the second column, and large in the third column. The wheels spin clockwise and travel to the right. $\tilde{t} \sim 57, 61, 119$, respectively, for the three shapes.

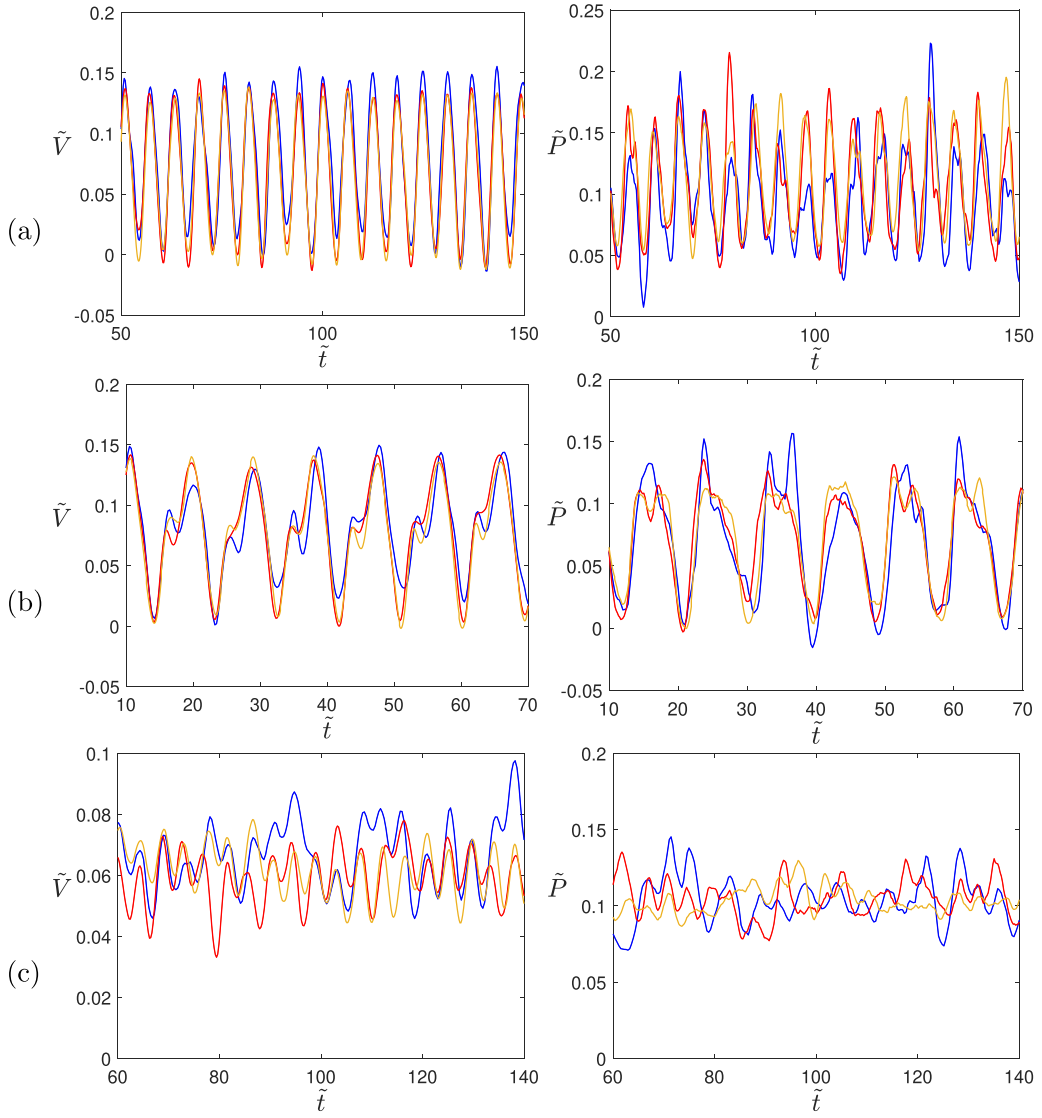

FIG. 6. Dimensionless power and traveling velocity comparisons of (a) a set of three triangle wheels, (b) a set of rectangle wheels, and (c) a set of hexagonal wheels on horizontal beds of cohesive particles. Blue curves stand for small wheels, red curves for medium wheels, and yellow curves for large wheels.

From the numerical standpoint, we reiterate that there are many types of cohesive interactions possible, and we are considering only a simple, van der Waals-type medium-range interaction here. Though the interactions and flow behaviours of cohesive granular materials are more complicated than noncohesive, the results presented here suggest that a simple scaling law exists to predict the driving performance of wheels on cohesive granular beds, as long as the cohesive length scale is small enough that a characteristic cohesion strength σ_c is the only relevant variable.

VI. CONCLUSION

In this work, scaling relations for driving performance, namely, the power and traveling velocity, have been proposed for wheeled locomotion on inclined and cohesive granular beds. For verification, DEM simulations of different shaped wheels have been performed, and the results have confirmed the proposed scaling relations. These scaling relations shed light on how to design experiments in laboratory scales and/or in a different gravitational environment by following the dimensionless groups. For example, consider two driving experiments in the same (noncohesive) grains having common wheel shape f, where one system has inputs $(g, L, M, D_W, \omega, \theta)$ and the other has $(g', L', M', D'_W, \omega', \theta') \equiv (qg, rL, sM, sr^{-2}D_W, q^{1/2}r^{-1/2}\omega, \theta)$, where q, r, s are arbitrary scalars that can be selected by the user. Then, by Eq. (1), these two tests have matching dimensionless inputs and ought to obey similitude. If the grains used in the pair of tests are also cohesive, Eq. (1) would now require $r = 1/q$ in order to secure dynamic similarity, thereby removing one free parameter from the design space for the scaled test. However, if σ_c can be tuned in the locomotion experiments, then three free parameters reemerge in the cohesive case. Because the scalings were obtained assuming a local granular rheology, they are more accurate when the grain size is indeed negligible compared with wheel length scales, since small-body intrusion effects may bring out rheologically nonlocal contributions in the granular media. For example, wheels with vary narrow features or wheels that do not protrude into the bed deeply enough compared to the grain size may not satisfy the scalings as well. In this work, we have studied the two factors (cohesion and inclination) individually, to provide a controlled and systematic study of those effects. Our results leave us encouraged that the locomotive scalings will continue to function on beds that are both inclined *and* cohesive, though direct validation of this is left as future work. To do so would require performing simulations over a wide sweep of input space, varying wheel shapes, sizes, cohesion, and inclination, which requires a fairly sizable amount of computational resources, especially considering cohesive particles are more computationally expensive.

ACKNOWLEDGMENT

Q.Z., S.T., and K.K. gratefully acknowledge support from Army Research Office grants W911NF1510196, W911NF1810118, and W911NF1610440 .

[1] S. S. Sharpe, Y. Ding, and D. I. Goldman, Environmental interaction influences muscle activation strategy during sand-swimming in the sandfish lizard *Scincus scincus*, J. Exp. Biol. **216**, 260 (2013).

[2] A. G. Winter, R. L. Deits, and A. E. Hosoi, Localized fluidization burrowing mechanics of *Ensis directus*, J. Exp. Biol. **215**, 2072 (2012).

[3] P. E. Schiebel, H. C. Astley, J. M. Rieser, S. Agarwal, C. Hubicki, A. M. Hubbard, K. Diaz, J. R. Mendelson III, K. Kamrin, and D. I. Goldman, Mitigating memory effects during undulatory locomotion on hysteretic materials, eLife **9**, e51412 (2020).

[4] J. Wong, M. Garber, and J. Preston-Thomas, Theoretical prediction and experimental substantiation of the ground pressure distribution and tractive performance of tracked vehicles, Proc. Inst. Mech. Eng. D **198**, 265 (1984).

[5] A. Brucks, T. Arndt, J. M. Ottino, and R. M. Lueptow, Behavior of flowing granular materials under variable *g*, Phys. Rev. E **75**, 032301 (2007).

[6] E. Altshuler, H. Torres, A. González-Pita, G. Sánchez-Colina, C. Pérez-Penichet, S. Waitukaitis, and R. Hidalgo, Settling into dry granular media in different gravities, Geophys. Res. Lett. **41**, 3032 (2014).

[7] Y. Ding, S. S. Sharpe, A. Masse, and D. I. Goldman, Mechanics of undulatory swimming in a frictional fluid, PLoS Comput. Biol. **8**, e1002810 (2012).

[8] F. Guillard, Y. Forterre, and O. Pouliquen, Lift forces in granular media, Phys. Fluids **26**, 043301 (2014).

[9] M. G. Bekker, *Theory of Land Locomotion* (University of Michigan Press, Ann Arbor, 1956).

[10] J. Y. Wong, *Terramechanics and Off-Road Vehicles* (Elsevier, Amsterdam, Netherlands, 1989).
[11] R. B. Ahlvin and P. W. Haley, *NATO reference mobility model: Edition II, NRMM user's guide* (US Army Engineer Waterways Experiment Station, Vicksburg, 1992).
[12] G. I. Taylor, Analysis of the swimming of microscopic organisms, Proc. R. Soc. Lond. A **209**, 447 (1951).
[13] S. Agarwal, C. Senatore, T. Zhang, M. Kingsbury, K. Iagnemma, D. I. Goldman, and K. Kamrin, Modeling of the interaction of rigid wheels with dry granular media, J. Terramechanics **85**, 1 (2019).
[14] C. Li, T. Zhang, and D. I. Goldman, A terradynamics of legged locomotion on granular media, Science **339**, 1408 (2013).
[15] H. Askari and K. Kamrin, Intrusion rheology in grains and other flowable materials, Nat. Mater. **15**, 1274 (2016).
[16] A. Schofield and P. Wroth, *Critical State Soil Mechanics* (McGraw-Hill, London, 1968).
[17] D. M. Wood, *Soil Behaviour and Critical State Soil Mechanics* (Cambridge University Press, Cambridge, 1990).
[18] S. Roux and F. Radjai, in Physics of Dry Granular Media, edited by H. J. Herrmann, J. P. Hovi, and S. Luding (Springer, New York, 1998), pp. 229–236.
[19] T. S. Majmudar and R. P. Behringer, Contact force measurements and stress-induced anisotropy in granular materials, Nature (London) **435**, 1079 (2005).
[20] GDR MiDi, On dense granular flows, Eur. Phys. J. E **14**, 341 (2004).
[21] F. da Cruz, S. Emam, M. Prochnow, J.-N. Roux, and F. Chevoir, Rheophysics of dense granular materials: Discrete simulation of plane shear flows, Phys. Rev. E **72**, 021309 (2005).
[22] P. Jop, Y. Forterre, and O. Pouliquen, A constitutive law for dense granular flows, Nature (London) **441**, 727 (2006).
[23] K. Kamrin and G. Koval, Nonlocal Constitutive Relation for Steady Granular Flow, Phys. Rev. Lett. **108**, 178301 (2012).
[24] K. Kamrin and D. L. Henann, Nonlocal modeling of granular flows down inclines, Soft Matter **11**, 179 (2015).
[25] B. Kou, Y. Cao, J. Li, C. Xia, Z. Li, H. Dong, A. Zhang, J. Zhang, W. Kob, and Y. Wang, Granular materials flow like complex fluids, Nature (London) **551**, 360 (2017).
[26] J. Slonaker, D. C. Motley, Q. Zhang, S. Townsend, C. Senatore, K. Iagnemma, and K. Kamrin, General scaling relations for locomotion in granular media, Phys. Rev. E **95**, 052901 (2017).
[27] S. S. Sharpe, R. Kuckuk, and D. I. Goldman, Controlled preparation of wet granular media reveals limits to lizard burial ability, Phys. Biol. **12**, 046009 (2015).
[28] R. Jewel, A. Panaitescu, and A. Kudrolli, Micromechanics of intruder motion in wet granular medium, Phys. Rev. Fluids **3**, 084303 (2018).
[29] In three dimensions there are several choices one could make for the directionality (such as codirectionality vs double shearing) and the definition of τ (such as Tresca's equivalent stress vs equivalent shear stress) and p (such as the normal stress on the flow plane vs the hydrostatic stress). But for any choice of the definitions, the same scaling laws come out as long as the model remains isotropic.
[30] R. Shield, On Coulomb's law of failure in soils, J. Mech. Phys. Solids **4**, 10 (1955).
[31] M. Massoudi and M. Mehrabadi, A continuum model for granular materials: Considering dilatancy and the Mohr-Coulomb criterion, Acta Mech. **152**, 121 (2001).
[32] R. M. Nedderman, *Statics and Kinematics of Granular Materials* (Cambridge University Press, Cambridge, 2005).
[33] R. C. Hurley and J. E. Andrade, Continuum modeling of rate-dependent granular flows in SPH, Comput. Particle Mech. **4**, 119 (2017).
[34] D. L. Henann and K. Kamrin, A predictive, size-dependent continuum model for dense granular flows, Proc. Natl. Acad. Sci. USA **110**, 6730 (2013).
[35] A. Thoesen, T. McBryan, M. Green, D. Mick, J. Martia, and H. Marvi, Revisiting scaling laws for robotic mobility in granular media, IEEE Robot. Autom. Lett. **5**, 1319 (2020).
[36] S. Dunatunga and K. Kamrin, Continuum modeling of projectile impact and penetration in dry granular media, J. Mech. Phys. Solids **100**, 45 (2017).

[37] A. H. Clark, A. J. Petersen, L. Kondic, and R. P. Behringer, Nonlinear Force Propagation during Granular Impact, Phys. Rev. Lett. **114**, 144502 (2015).
[38] S. Plimpton, Fast parallel algorithms for short-range molecular dynamics, J. Comput. Phys. **117**, 1 (1995).
[39] G. Koval, J.-N. Roux, A. Corfdir, and F. Chevoir, Annular shear of cohesionless granular materials: From the inertial to quasistatic regime, Phys. Rev. E **79**, 021306 (2009).
[40] K. Kamrin and G. Koval, Effect of particle surface friction on nonlocal constitutive behavior of flowing granular media, Comput. Particle Mech. **1**, 169 (2014).
[41] Q. Zhang and K. Kamrin, Microscopic Description of the Granular Fluidity Field in Nonlocal Flow Modeling, Phys. Rev. Lett. **118**, 058001 (2017).
[42] S. T. Nase, W. L. Vargas, A. A. Abatan, and J. McCarthy, Discrete characterization tools for cohesive granular material, Powder Technol. **116**, 214 (2001).
[43] F. Bertrand, L.-A. Leclaire, and G. Levecque, DEM-based models for the mixing of granular materials, Chem. Eng. Sci. **60**, 2517 (2005).
[44] S. Luding, Contact models for very loose granular materials, in *IUTAM Symposium on Multiscale Problems in Multibody System Contacts*, edited by P. Eberhard (Springer, Dordrecht, Netherlands, 2007), pp. 135–150.
[45] R. D. Venkatesh, M. Grmela, and J. Chaouki, Simulations of vibrated fine powders, Powder Technol. **100**, 211 (1998).
[46] G. Lian, C. Thornton, and M. J. Adams, A theoretical study of the liquid bridge forces between two rigid spherical bodies, J. Colloid Interface Sci. **161**, 138 (1993).
[47] M. Toivakka, P. Salminen, Y. Chonde, and D. Bousfield, Consolidation of particulate suspension—Model study with plastic pigments, in *Proceedings of 1997 TAPPI Advanced Coating Fundamentals Symposium* (TAPPI Press Atlanta, 1997), p. 89.
[48] G. Grégoire, H. Chaté, and Y. Tu, Moving and staying together without a leader, Physica D **181**, 157 (2003).
[49] L. E. Silbert, J. W. Landry, and G. S. Grest, Granular flow down a rough inclined plane: Transition between thin and thick piles, Phys. Fluids **15**, 1 (2003).
[50] A. Janda, I. Zuriguel, A. Garcimartín, L. A. Pugnaloni, and D. Maza, Jamming and critical outlet size in the discharge of a two-dimensional silo, EPL (Europhys. Lett.) **84**, 44002 (2008).
[51] C. Lun, S. B. Savage, D. Jeffrey, and N. Chepurniy, Kinetic theories for granular flow: Inelastic particles in Couette flow and slightly inelastic particles in a general flowfield, J. Fluid Mech. **140**, 223 (1984).
[52] J. T. Jenkins and S. B. Savage, A theory for the rapid flow of identical, smooth, nearly elastic, spherical particles, J. Fluid Mech. **130**, 187 (1983).
[53] I. S. Aranson and L. S. Tsimring, Continuum theory of partially fluidized granular flows, Phys. Rev. E **65**, 061303 (2002).
[54] D. Volfson, L. S. Tsimring, and I. S. Aranson, Order Parameter Description of Stationary Partially Fluidized Shear Granular Flows, Phys. Rev. Lett. **90**, 254301 (2003).
[55] A. Gans, O. Pouliquen, and M. Nicolas, Cohesion-controlled granular material, Phys. Rev. E **101**, 032904 (2020).